MOLECULAR IMAGING AND BIOLOGY

RESEARCH ARTICLE

[11C]-DPA-713 and [18F]-DPA-714 as New PET Tracers for TSPO: A Comparison with [11C]-(R)-PK11195 in a Rat Model of Herpes Encephalitis

Janine Doorduin,[1] Hans C. Klein,[1,2] Rudi A. Dierckx,[1] Michelle James,[3]
Michael Kassiou,[3,4,5] Erik F. J. de Vries[1]

[1]Department of Nuclear Medicine and Molecular Imaging, University Medical Center Groningen, University of Groningen, P.O. Box 30.001, 9700 RB Groningen, The Netherlands
[2]University Center of Psychiatry, University Medical Center Groningen, University of Groningen, P.O. Box 30.001, 9700 RB Groningen, The Netherlands
[3]Brain and Mind Research Institute, University of Sydney, Camperdown, NSW 2050 Australia
[4]School of Chemistry, University of Sydney, Sydney, NSW 2006 Australia
[5]Discipline of Medical Radiation Sciences, University of Sydney, Sydney, NSW 2006 Australia

Abstract

Background: Activation of microglia cells plays an important role in neurological diseases. Positron emission tomography (PET) with [11C]-(R)-PK11195 has already been used to visualize activated microglia cells in neurological diseases. However, [11C]-(R)-PK11195 may not possess the required sensitivity to visualize mild neuroinflammation. In this study, we evaluated the PET tracers [11C]-DPA-713 and [18F]-DPA-714 as agents for imaging of activated microglia in a rat model of herpes encephalitis.
Materials and Methods: Rats were intranasally inoculated with HSV-1. On day 6 or 7 after inoculation, small animal PET studies were performed to compare [11C]-(R)-PK11195, [11C]-DPA-713, and [18F]-DPA-714.
Results: Uptake of [11C]-DPA-713 in infected brain areas was comparable to that of [11C]-(R)-PK11195, but [11C]-DPA-713 showed lower non-specific binding. Non-specific uptake of [18F]-DPA-714 was lower than that of [11C]-(R)-PK11195. In the infected brain, total [18F]-DPA-714 uptake was lower than that of [11C]-(R)-PK11195, with comparable specific uptake.
Conclusions: [11C]-DPA-713 may be more suitable for visualizing mild inflammation than [11C]-(R)-PK11195. In addition, the fact that [18F]-DPA-714 is an agonist PET tracer opens new possibilities to evaluate different aspects of neuroinflammation. Therefore, both tracers warrant further investigation in animal models and in a clinical setting.

Key words: Positron emission tomography, Neuroinflammation, Microglia, [11C]-PK11195, TSPO

Introduction

Neurological disorders are a significant burden to society worldwide, especially in countries where a growing proportion of the population is over 65 years old [1]. Despite the large difference between neurological disorders, neuroinflammation is involved in both acute pathology, such as stroke and herpes encephalitis, and chronic neurodegenerative diseases, such as Parkinson's and Alzheimer's disease. Although neuroinflammation was found to be involved in neurological disorders, it is still not known when the

Correspondence to: Janine Doorduin; *e-mail:* j.doorduin@ngmb.umcg.nl

inflammatory response is beneficial, detrimental, or incidental. Nakajima and Kohsaka [2] proposed that neuroinflammation in acute injuries is beneficial, whereas it will lead to neuronal cell death in chronic diseases. When the exact role of neuroinflammation in different neurological disorders is unraveled, this will inevitably lead to early diagnosis, possible therapeutic intervention, and improved treatment.

One of the key players in neuroinflammation is the microglia cell, which provides the first line of defense against brain tissue injuries. In the healthy central nervous system, microglia cells continuously survey their microenvironment by rapid extension and extraction of their ramified processes [3, 4]. In response to a wide variety of central nervous system insults, microglia cells become activated and change from their ramified state into amoeboid morphology. The activation of microglia cells is accompanied by an increased expression of the translocator protein (TSPO), an 18 kDa component of a heteromeric complex. The expression of the TSPO is low in the healthy brain, but is highly upregulated in neuroinflammation.

Positron emission tomography (PET) is a non-invasive imaging technique that can be used to study the role of neuroinflammation in neurological disorders, using the TSPO as a biomarker. PET has already been used in numerous clinical studies to visualize activated microglia cells using the isoquinoline [^{11}C]-(R)-PK11195 ((R)-N-methyl-N-(1-methylpropyl)-1-(2-chlorophenyl)isoquinoline-3-carboxamide) as the tracer. [^{11}C]-(R)-PK11195 is a ligand for the TSPO. Although [^{11}C]-(R)-PK11195 has already been used to image activated microglia cells in, among others, stroke [5–8], multiple sclerosis [9–12], herpes encephalitis [13], Parkinson's disease [14, 15], and Alzheimer's disease [16–18], it is not an ideal tracer, since it shows low brain uptake and high nonspecific binding. Pharmacokinetic modeling of the PET data is complicated and [^{11}C]-(R)-PK11195 may not possess the sensitivity to visualize mild neuroinflammation, which makes it unsuitable for use in early diagnosis and detection of subtle effects of therapeutic intervention.

Therefore, a more sensitive and specific PET tracer for TSPO imaging would be of great interest. Pyrazolopyrimidines display high affinity for the TSPO and two compounds from this class have already been radiolabeled for use in PET. The pyrazolopyrimidines DPA-713 and DPA-714 have higher affinity for the TSPO in vitro (Ki=4.7 nM and Ki=7.0 nM, respectively) than PK11195 (Ki=9.3 nM) [19–21]. The TSPO antagonist DPA-713 was labeled with carbon-11 and evaluated in vivo in a healthy baboon [22]. It was concluded that [^{11}C]-DPA-713 is a specific ligand for the TSPO and that it may be useful for studying changes in the density of TSPO binding sites. In addition, [^{11}C]-DPA-713 exhibited a higher signal-to-noise ratio than [^{11}C]-(R)-PK11195 in a rat model of neurodegeneration, which makes it more suitable for quantification of TSPO binding sites [23]. The TSPO agonist, DPA-714, was labeled with fluorine-18 and demonstrated good uptake in the primate brain and an eightfold higher uptake in the lesioned striatum of a quinolinic acid-lesioned rat model of activated microglia [19, 20]. This higher uptake was shown to be selective TSPO binding.

Both [^{11}C]-DPA-713 and [^{18}F]-DPA-714 have demonstrated better imaging properties than [^{11}C]-(R)-PK11195 in striatum-lesioned rats [19, 20, 23]. However, striatum lesion by injection of a toxic compound requires invasive manipulations to generate an inflammatory response. The aim of this study was to validate these tracers in a different rat model that does not require invasive manipulation and unnatural toxic compounds to evoke neuroinflammation, which may better mimic microglia activation in neurological disorders. Therefore, [^{11}C]-DPA-713 and [^{18}F]-DPA-714 were evaluated in a rat model of herpes encephalitis (HSE) and compared to [^{11}C]-(R)-PK11195.

Materials and Methods

[^{11}C]-(R)-PK11195

[^{11}C]-(R)-PK11195 was labeled by trapping [^{11}C]-methyl iodide [24] in a solution of 1 mg (R)-N-desmethyl PK11195 and 10 mg potassium hydroxide in 300 µl dimethylsulfoxide. The reaction mixture was allowed to react for 1 min at 40°C, neutralized with 1 M HCl, and passed through a 45-µm Millex HV filter. The filtrate was purified by high-performance liquid chromatography (HPLC) using a µBondapak C18 column (7.8×300 mm) with acetonitrile/25 mM NaH$_2$PO$_4$ (pH 3.5) (55/45) as the eluent (flow 5 ml/min). To remove the organic solvents from the product, the collected HPLC fraction (retention time 7 min) was diluted with 100 ml of water and passed through an Oasis HLB 30 mg (1 cc) cartridge. The cartridge was washed twice with 10 ml of water and subsequently eluted with 0.7 ml of ethanol and 5 ml of water. The product was sterilized by filtration over a 22 µm Millex LG filter. The product was obtained in 33±15% radiochemical yield (n=11). Quality control was performed by HPLC, using a Novapak C18 column (150×3.9 mm) with acetonitrile/25 mM NaH$_2$PO$_4$ (pH 3.5; 60/40) as the eluent at a flow of 1 ml/min. The radiochemical purity was always >95% and the specific activity was 51±18 MBq/nmol.

[^{11}C]-DPA-713 (Compound 2)

For the preparation of N,N-diethyl-2-(2-(4-[^{11}C]methoxyphenyl)-5,7-dimethylpyrazolo(1,5-α)pyrimidin-3-yl)acetamide (compound 2, [^{11}C]DPA-713), [^{11}C]-methyl triflate was trapped in a solution of 1 mg N,N-diethyl-2-(2-(4-hydroxyphenyl)-5,7-dimethylpyrazolo(1,5-α)pyrimidin-3-yl)acetamide (compound 1) [22] and 2.5 µl 0.5 M NaOH in 0.5 ml of acetonitrile (Fig. 1). After 5 min at 100°C, the reaction mixture was diluted with 0.5 ml of acetonitrile and 1 ml of water and purified by HPLC using a SymmetryPrep C18 column (7 µm, 7.8×300 mm) and acetonitrile/0.1 M NaH$_2$PO$_4$ (1/1) as the eluent (flow 5 ml/min). The radioactive product with a retention time of 7–8 min was collected. The product was diluted with 100 ml of water and passed through an Oasis HLB 30 mg (1 cc) cartridge. The cartridge was washed twice with 10 ml of water and subsequently eluted with 0.7 ml of ethanol and 5 ml of water. The product was sterilized by filtration over a 22-µm Millex LG filter. The product is obtained in 48±15% radiochemical yield (n=10). Quality control was performed by HPLC, using a Novapak C18 column (150×3.9 mm) with acetonitrile/25 mM NaH$_2$PO$_4$ (40/60) as the eluent at a flow of 1 ml/min. The radiochemical purity of [^{11}C]DPA-713 was always >99% and the specific activity was 41±12 MBq/nmol.
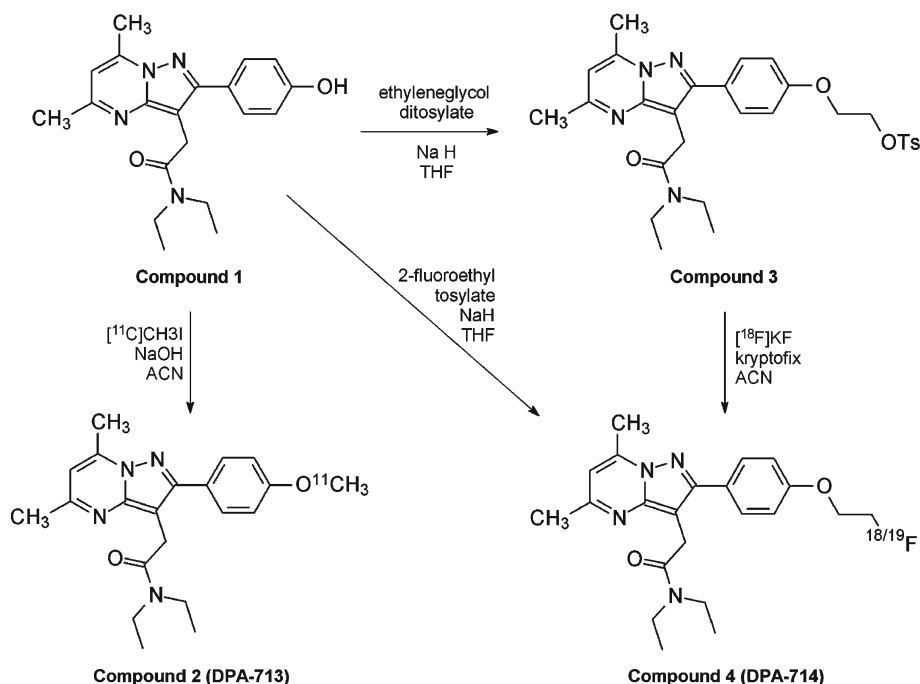
Fig. 1. Synthesis of DPA-713 from the labeling precursor compound 1 and DPA-714 from the labeling precursor compound 3. The labeling precursor compound 3 and the reference material for DPA-714 were synthesized from compound 1 using ethyleneglycol ditosylate and 2-fluoroethyltosylate as the alkylating agent, respectively.

N,N-diethyl-2-(2-(4-[2-tosyloxy-1-ethoxy]phenyl)-5,7-dimethylpyrazolo(1,5-α)pyrimidin-3-yl) acetamide (Compound 3)

To a suspension of 42 mg 55% NaH (1.0 mmol) in 15 ml freshly distilled tetrahydrofuran (THF), 100 mg (0.44 mmol) of N,N-diethyl-2-(2-(4-hydroxyphenyl)-5,7-dimethylpyrazolo(1,5-α)pyrimidin-3-yl)acet-amide (compound 1) [22] was added (Fig. 1). After the reaction mixture was refluxed for 30 min, a solution of 300 mg (0.87 mmol) ethyl-eneglycol ditosylate in 20 ml THF was quickly added to the hot reaction mixture. After another 18 h of refluxing, the reaction flask was cooled on ice and the reaction was quenched by slowly adding 50 ml of water. The mixture was extracted three times with 25 ml of dichloromethane. The combined organic layers were washed with 50 ml of water, dried on anhydrous sodium sulfate, and filtered. The product was purified by flash column chromatography (silica gel), using 3% methanol in dichloromethane as the eluent. The product was obtained as a light yellow solid in 59% yield (140 mg). ^{1}H-NMR (CDCl$_3$, 200 MHz): δ 7.83 (d, 2H, J=8.1 Hz, tosyl), 7.74 (d, 2H, J=8.8 Hz, Ar), 7.35 (d, 2H, J=8.1 Hz, tosyl), 6.86 (d, 2H, J=8.8 Hz, Ar), 6.52 (s, 1H, Ar), 4.39 (t, 2H, J=4.6 Hz, CH$_2$O), 4.19 (t, 2H, J=4.6 Hz, CH$_2$O), 3.95 (s, 2H, CH$_2$C=O), 3.51 (q, 2H, J=7.1 Hz, CH$_2$N), 3.40 (q, 2H, J=7.1 Hz, CH$_2$N), 2.75 (s, 3H, CH$_3$), 2.58 (s, 3H, CH$_3$), 2.45 (s, 3H, tosyl), 1.21 (t, 3H, J=7.1 Hz, CH$_2$*CH$_3$*), 1.11 (t, 3H, J=7.1 Hz, CH$_2$*CH$_3$*).

N,N-diethyl-2-(2-(4-[2-fluoro-1-ethoxy]phenyl)-5,7-dimethylpyrazolo(1,5-α)pyrimidin-3-yl) acetamide (Compound 4, DPA-714)

Reference material of DPA-714 (compound 4) was prepared as described for compound 3, except 2-fluoroethyl tosylate was used as the alkylating agent instead of ethyleneglycol ditosylate (Fig. 1). Yield was 80% (light yellow solid). ^{1}H-NMR (CDCl$_3$, 200 MHz): δ 7.74 (d,

2H, J=8.1 Hz, Ar), 6.99 (d, 2H, J=8.1 Hz, Ar), 6.54 (s, 1H, Ar), 4.77 (dd, 2H, J=2.9 Hz, J=47.6 Hz, CH$_2$F), 4.26 (dd, 2H, J=2.9 Hz, J=27.5 Hz, CH$_2$O), 4.05 (s, 2H, CH$_2$C=O), 3.51 (q, 2H, J=7.0 Hz, CH$_2$N), 3.41 (q, 2H, J=7.0 Hz, CH$_2$N), 2.78 (s, 3H, CH$_3$), 2.64 (s, 3H, CH$_3$), 1.23 (t, 3H, J=7.0 Hz, CH$_2$*CH$_3$*), 1.12 (t, 3H, J=7.0 Hz, CH$_2$*CH$_3$*).

$[^{18}F]$-DPA-714 ($[^{18}F]$-Compound 4)

$[^{18}F]$Fluoride was eluted from a Waters QMA anion exchange cartridge with 5 mg potassium carbonate in 1 ml of water and collected into a vial containing 20 mg kryptofix[2.2.2]. $[^{18}F]$KF/kryptofix[2.2.2] was dried by azeotropic distillation with acetoni-trile at 130°C. A solution of 1 mg compound 3 in 0.5 ml dry DMF was added to the $[^{18}F]$KF/kryptofix complex. The reaction mixture was allowed to react for 10 min at 100°C. After cooling, the reaction mixture was diluted with water and HPLC eluent (acetonitrile/0.1 M NaH$_2$PO$_4$ (45/55)) and passed through an Alumina N seppak to remove the majority of unreacted $[^{18}F]$ fluoride. The product was purified by HPLC using a SymmetryPrep C18 column (7 µm, 7.8×300 mm) with acetonitrile/0.1 M NaH$_2$PO$_4$ (45/55) as the eluent (flow 5 ml/min). To remove the organic solvents from the product, the collected HPLC fraction (retention time 11 min) was diluted with 15 ml of water and passed through an Oasis HLB 30 mg (1 cc) cartridge. The cartridge was washed with 5 ml of water and subsequently eluted with 0.7 ml of ethanol and 5 ml of water. The product was sterilized by filtration over a 22-µm Millex LG filter. The product was obtained in 17±8% radiochemical yield. Quality control was performed by HPLC, using a Novapak C18 column (150×3.9 mm) with acetonitrile/25 mM NaH$_2$PO$_4$ (35/65) as the eluent at a flow of 1 ml/min. The radiochemical purity was >99% and the specific activity was 80±35 MBq/nmol (n=11).

Animals

Male outbred Wistar-Unilever (SPF) rats (weight 287±38 g) were obtained from Harlan (Lelystad, The Netherlands). The rats were individually housed in Macrolon cages (38×26×24 cm) on a layer of wood shavings in a room with constant temperature (21±2°C) and fixed, 12-h light–dark regime. Food (standard laboratory chow, RMH-B, Hope Farms, The Netherlands) and water were available *ad libitum*. After arrival, the rats were allowed to acclimatize for at least 7 days. The rats were randomly divided into nine groups: control rats (control) scanned with either [11C]-(R)-PK11195 (n=5), [11C]-DPA-713 (n=5), or [18F]-DPA-714 (n=5), rats infected with HSV-1 (HSE) scanned with either [11C]-(R)-PK11195 (n=9), [11C]-DPA-713 (n=9), or [18F]-DPA-714 (n=9), and rats infected with HSV-1 and pre-treated with PK11195 (HSE pre-treated with PK11195) scanned with either [11C]-(R)-PK11195 (n=4), [11C]-DPA-713 (n=4), or [18F]-DPA-714 (n=4). After PET scanning, the rats were killed and the ex vivo biodistribution of the tracers was determined. The study was approved by the Animal Ethics Committee of the University of Groningen, The Netherlands.

HSV-1 Inoculation

The HSV-1 strain was obtained from a clinical isolate, cultured in Vero cells and assayed for plaque forming units (PFU) per milliliter. The rats were slightly anaesthetized with 5% isoflurane (Pharmachemie BV, The Netherlands) and inoculated with HSV-1 by the application of 100 μl of phosphate-buffered saline (PBS) with 1×10^7 PFU of virus on the nostrils (50 μl per nostril) with a micropipette. Control rats were treated similarly by the application of 100 μl PBS without virus. Clinical symptoms in all rats were scored daily after the inoculation by the same observer.

Immunohistochemistry

Immunohistochemical staining was performed in control and HSV-1-infected rats on day 7 after inoculation. The rats were euthanized and the brains were removed and frozen at −80°C. Coronal brain sections of 10 μm were cut at −18°C using a cryostat (Leica Microsystems, Germany). Sections were collected on slides, vacuum-dried, fixated for 20 min in paraformaldehyde (4% in 100 nM PBS), and washed three times for 5 min in 100 nM PBS. To block non-specific binding, sections were incubated with 5% normal goat serum in PBS containing 3% triton and washed for 5 min in 100 nM PBS. Sections were incubated overnight at 4°C with the primary antibody (Anti Iba1 Rabbit (1:750), Wako Chemicals, USA). After incubation, sections were washed three times for 5 min in 100 nM PBS and incubated for 1 h with the secondary antibody (FITC-conjugated Goat Anti Rabbit IgG (1:250), Jackson ImmunoResearch Laboratories Inc., USA) in 1% normal goat serum in PBS containing 3% triton. As a negative control, sections were only incubated with the secondary antibody. Subsequently, sections were washed three times for 5 min in PBS and mounted with Mowiol mounting medium. The fluorescence was examined by using a microscope (Zeiss Axioskop 2, Carl Zeiss Microimaging Inc., Germany) in combination with the Leica Application Suite (Version 2.3.3 R1, Leica, Germany).

PET Studies

PET scans were performed when robust clinical signs of infection appeared, which was either on day 6 or on day 7 after the inoculation with HSV-1. The rats were anesthesized by an intraperitoneal injection of medetomidine (Domitor, Pfizer, The Netherlands, 0.2 mg/kg) and ketamine (Ketanest, Pfizer, The Netherlands, 25 mg/kg), after which the rats were positioned in the small animal PET camera (Focus 220, Siemens Medical Solutions USA, Inc.) in transaxial position with their heads in the field of view. A transmission scan of 515 s with a Co-57 point source was obtained for the correction of attenuation by tissue. After the transmission scan was completed, the PET tracer [11C]-(R)-PK11195 (65±22 MBq, 0.71±0.48 μg), [11C]-DPA-713 (82±23 MBq, 0.91±0.31 μg), or [18F]-DPA-714 (37±12 MBq, 0.36±0.18 μg) was injected via the penile vein. Simultaneous with the injection of the PET tracer, an emission scan of 62 min was started for [11C]-(R)-PK11195 and [11C]-DPA-713, and a PET scan of 120 min for [18F]-DPA-714. In the pre-treated group, unlabeled PK11195 (Sigma-Aldrich, USA, 5 mg/kg in dimethylsulfoxide at a concentration of 10 mg/ml) was administered via the tail vein 5 min prior to injection of the PET tracer.

The list-mode data of the emission scans was separated into 21 frames (8×30, 3×60, 2×120, 2×180, 3×300, and 3×600 s) for [11C]-(R)-PK11195 and [11C]-DPA-713, and into 28 frames for [18F]-DPA-714 (8×30, 4×60, 3×120, 2×180, 4×300, and 8×600 s). Emission sinograms were iteratively reconstructed (OSEM2d, four iterations) after being normalized, corrected for attenuation, and corrected for decay of radioactivity.

PET Image Analysis

PET image analysis was performed using the Clinical Applications Packaging Program (CAPP5). Regions of interest were drawn around the bulbus olfactorius, frontal cortex, striatum, parietal/temporal/occipital cortex, brainstem, and cerebellum in a template PET scan that was co-registered with the PET scan of interest by image fusion. The time–activity curves per region of interest were determined in becquerel per cubic centimeter units and converted into standardized uptake values (SUV), defined as: [tissue activity concentration (MBq/g)]/[(injected dose (MBq)/body weight (g)]. It was assumed that 1 cm^3 of brain tissue equals 1 g. To correct for the activity in plasma, each point on the time–activity curve (SUV) was divided by the ex vivo plasma uptake (SUV) at t=60 min for [11C]-(R)-PK11195 and [11C]-DPA-713, and at $t=120$ min for [18F]-DPA-714 creating a tissue/plasma ratio.

Ex Vivo Biodistribution

After the PET scan, the rats were killed by extirpation of the heart while under deep anesthesia. The brain was dissected into several brain areas, peripheral organs were excised, and blood was centrifuged to collect a plasma sample. The brain areas, peripheral organs, and plasma were weighed and analyzed for the amount of radioactivity by using a gammacounter (LKB Wallac, Turku, Finland). Tracer uptake is expressed as the SUV.

To correct for activity of the tracers in plasma, the tissue/plasma ratio was calculated by dividing the uptake (SUV) in the different brain areas by the plasma uptake (SUV), for all rats individually. Subsequently, the TSPO-specific uptake was calculated for control and HSE rats. The specific uptake was calculated by subtracting the average tissue/plasma ratio of the HSE rats pre-treated with PK11195 from the tissue/plasma ratio of control and HSE rats, for each rat individually.

Statistical Analysis

All data are expressed as mean ± standard deviation. Statistical analysis was performed using SPSS for Windows, version 14.0.2. Statistical analysis on differences between the uptake of $[^{11}C]$-(R)-PK11195, $[^{11}C]$-DPA-713, and $[^{18}F]$-DPA-714, which were obtained from the PET scan, was performed by one-way ANOVA. Per brain area, a Bonferonni post hoc test was used to determine if there were differences in uptake between the PET tracers. For the ex vivo biodistribution, statistical analysis on differences in uptake between control rats, HSE rats, and HSE rats pre-treated with PK11195 was performed by one-way ANOVA, using a Bonferonni post hoc test to compare the three conditions per brain area. Statistical analysis on differences between non-specific and specific uptake of $[^{11}C]$-(R)-PK11195, $[^{11}C]$-DPA-713, and $[^{18}F]$-DPA-714 was performed by one-way ANOVA, using a Bonferonni post hoc test to compare the uptake of the PET tracers per brain area. The time–activity curves were analyzed with the repeated measures general linear model of SPSS (version 14.0.2) using a Bonferroni post hoc test per brain area. Correlations of specific binding in control rats for $[^{11}C]$-(R)-PK11195, $[^{11}C]$-DPA-713, and $[^{18}F]$-DPA-714 with $[^{3}H]$-PK11195 binding as determined by Kurumaji et al. [25] were assessed with Pearson's product moment correlation coefficient (r). Significance was reached when the p value was <0.05.

Results

Clinical Symptoms

Clinical symptoms were scored daily up to 7 days post-inoculation and categorized into the following clinical scores: (0), no symptoms; (1), ruffled fur and irritated mouth, nose, and eyes; (2), behavioral signs, like stress and lethargy, and hunched posture; (3), posterior paralysis and impairment of motor function; and (4), severe paralysis, labored breathing or death. The first clinical symptoms in the HSE rats were seen on day 4 or 5 after inoculation with HSV-1, after which the severity of the symptoms increased. For both $[^{11}C]$-(R)-PK11195 and $[^{11}C]$-DPA-713, most rats had a score of 2 at the day of scanning, whereas most rats scanned with $[^{18}F]$-DPA-714 had a score of 3. The average of the scores (2.44±0.73 for $[^{11}C]$-(R)-PK11195, 2.11±0.78 for $[^{11}C]$-DPA-713 and 2.67±0.71 for $[^{18}F]$-DPA-714) did not differ significantly between groups. None of the control rats showed any clinical symptoms.
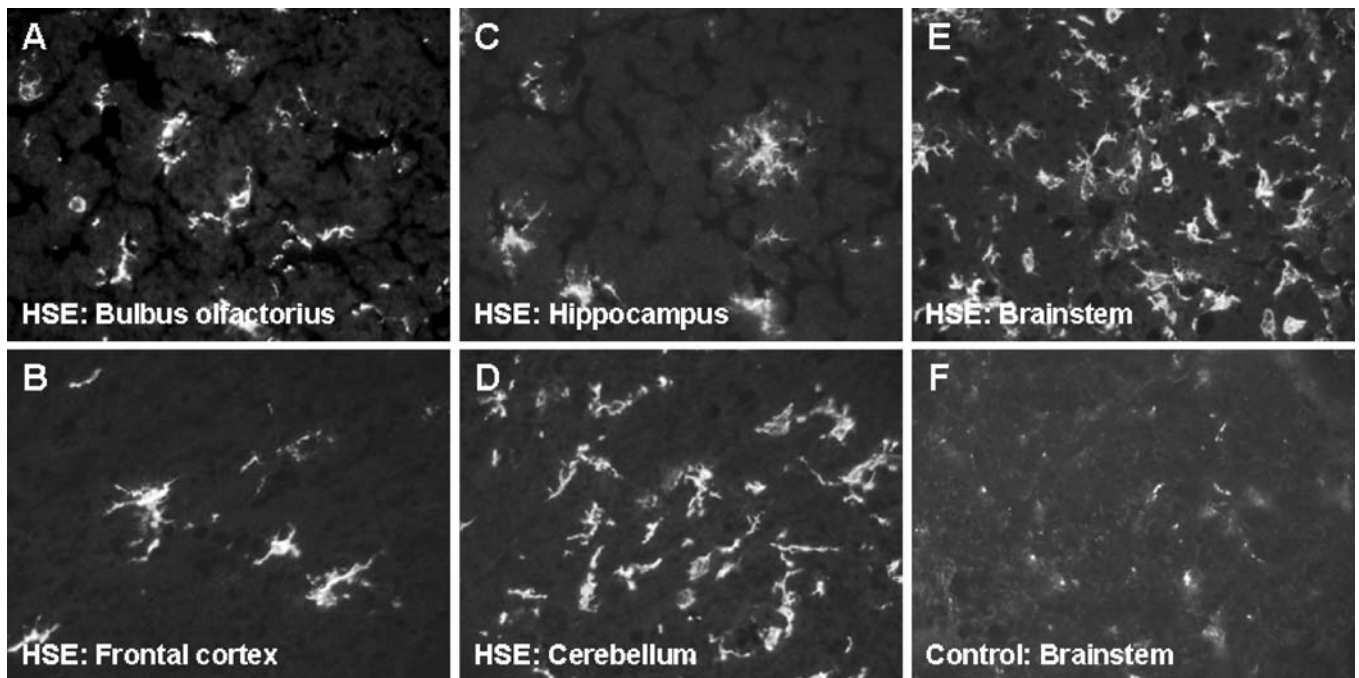
Immunohistochemistry

At day 7 after inoculation with HSV-1, intense microglial activation was observed in the bulbus olfactorius, cerebellum, and brainstem (Fig. 2). In addition, mild microglial activation was also seen in the frontal cortex and hippocampus of HSV-1-infected rats. The activated microglia cells could be recognized by the rounded shape with short processes, showing that the microglia cells had converted to the macrophage-like state. Microglial activation in the brainstem was observed throughout the whole brainstem and could not

be attributed to a specific area. In control rats, only ramified, resting microglia cells were observed in all brain areas.

Small Animal PET Imaging

The standardized uptake values obtained from the last 10 min of the PET scans are displayed in Table 1. The uptake of $[^{11}C]$-(R)-PK11195 in the last 10 min of the scan was significantly higher in the bulbus olfactorius, frontal cortex, parietal/temporal/occipital cortex, cerebellum, and brainstem in HSE rats when compared to control rats. The uptake was consistent with the immunohistochemistry data. The $[^{11}C]$-(R)-PK11195 uptake in the rats pre-treated with PK11195 was significantly decreased in the bulbus olfactorius, cerebellum, and brainstem. For $[^{11}C]$-DPA-713, a significant increase in tracer uptake was found in the brainstem and a non-significant increase in the bulbus olfactorius of HSE rats, as compared to control rats. Also, $[^{11}C]$-DPA-713 showed a statistically significant reduction in uptake by pre-treatment with PK11195 in the bulbus olfactorius, frontal cortex, parietal/temporal/occipital cortex, cerebellum and brainstem. The uptake of $[^{18}F]$-DPA-714 derived from the PET scan was found to be non-significantly higher in the bulbus olfactorius and brainstem in HSE rats, as compared to control rats. No effective blocking of $[^{18}F]$-DPA-714 by pre-treatment with PK11195 was found. The PET scan of $[^{18}F]$-DPA-714 was 120 min, while the PET scan of both $[^{11}C]$-(R)-PK11195 and $[^{11}C]$-DPA-713 was 60 min. For comparison, the uptake $[^{18}F]$-DPA-714 was also determined at 60 min, but no statistically significant differences were found between the uptake of $[^{18}F]$-DPA-714 at 60 and 120 min.

The time–activity curves of the brainstem are displayed in Fig. 3, to show the kinetics of the tracer over time. These time–activity curves were normalized for activity in plasma because tracer uptake in the brain is dependent on the tracer delivery from plasma. A change in plasma activity concentration due to, for example, pre-treatment with PK11195 can thus influence brain uptake. For plasma activity normalization, the uptake (SUV) on each individual time point was divided by the activity in plasma (SUV) as determined ex vivo on $t=60$ for $[^{11}C]$-(R)-PK11195 and $[^{11}C]$-DPA-713, and on $t=120$ for $[^{18}F]$-DPA-714. Post hoc analysis of the repeated measures general linear model revealed that the time–activity curve of $[^{11}C]$-(R)-PK11195 in the brainstem of HSE rats was significantly higher than that of control rats ($p<0.005$) and rats pre-treated with PK11195 ($p<0.005$). For $[^{11}C]$-DPA-713, the time–activity curve in HSE rats was significantly higher than in the control rats ($p<0.05$) and in rats pre-treated with PK11195 ($p<0.005$). In addition, the uptake of $[^{11}C]$-DPA-713 over time was significantly reduced by pre-treatment with PK11195, even when compared to control rats ($p<0.05$). No differences in time–activity curves of control, HSE, and pre-treated rats were found for $[^{18}F]$-DPA-714 in the brainstem, although pre-treatment with PK11195 non-significantly reduced the uptake in the brainstem.

Fig. 2. Images (×400) of immunohistochemical staining of microglia cells with Iba, on day 7 after inoculation. For rats infected with HSV-1 (*HSE*) microglia are shown in the bulbus olfactorius, frontal cortex, hippocampus, cerebellum, and brainstem (**a–e**). For control rats, only the brainstem (**f**) is shown. The staining in this brain area is representative for the staining in all other brain areas of control rats.

Ex Vivo Biodistribution: SUV

An ex vivo biodistribution study of the three PET tracers was performed to confirm the results of the PET studies. In addition, biodistribution allows investigation of uptake in smaller brain areas than is possible with small animal PET imaging. The ex vivo biodistribution, expressed as mean SUV ± SD, was consistent with the results obtained from the PET images. Uptake of $[^{11}C]$-(R)-PK11195 (Table 2) in the bulbus olfactorius was increased in HSE rats as compared to control rats (1.59 vs. 1.20); however, this increase did not reach statistical significance. A significant increase of $[^{11}C]$-

Table 1. Standardized uptake values (mean ± SD) obtained from the last 10 min of the PET scan of $[^{11}C]$-(R)-PK11195, $[^{11}C]$-DPA-713, and $[^{18}F]$-DPA-714 in control rats (control; $n=5$), rats infected with HSV-1 (HSE; $n=9$) and rats infected with HSV-1 pre-treated with 5 mg/kg PK11195 5 min before tracer injection (HSE + PK11195; $n=5$)

	$[^{11}C]$-(R)-PK11195	$[^{11}C]$-DPA-713	$[^{18}F]$-DPA-714
Control			
Brainstem	0.50±0.11	0.65±0.17	0.51±0.16
Bulbus olfactorius	0.70±0.16	0.74±0.20	0.57±0.18
Cerebellum	0.41±0.06	0.47±0.03	0.39±0.04
Frontal cortex	0.45±0.07	0.44±0.17	0.30±0.10
Parietal/temporal/occipital cortex	0.35±0.09	0.41±0.08	0.31±0.05
Striatum	0.29±0.07	0.29±0.06	0.19±0.04
HSE			
Brainstem	1.52±0.33**	1.23±0.42*	0.84±0.45
Bulbus olfactorius	1.29±0.33**	1.10±0.30	0.82±0.30
Cerebellum	1.02±0.24**	0.82±0.33	0.41±0.22
Frontal cortex	0.74±0.19*	0.60±0.13	0.41±0.18
Parietal/temporal/occipital cortex	0.54±0.14*	0.44±0.12	0.32±0.09
Striatum	0.47±0.13	0.34±0.11	0.23±0.06
HSE + PK11195			
Brainstem	0.76±0.04****	0.27±0.11****	0.44±0.07
Bulbus olfactorius	0.59±0.07****	0.33±0.10****	0.66±0.20
Cerebellum	0.64±0.09***	0.26±0.07***	0.48±0.05
Frontal cortex	0.62±0.07	0.27±0.10****	0.46±0.13
Parietal/temporal/occipital cortex	0.56±0.06	0.21±0.05*, ***	0.44±0.07*, ***
Striatum	0.61±0.12*	0.20±0.06	0.37±0.09**, ***

*$p<0.05$ as compared to control, **$p<0.005$ as compared to control, ***$p<0.05$ as compared to HSE, ****$p<0.005$ as compared to HSE
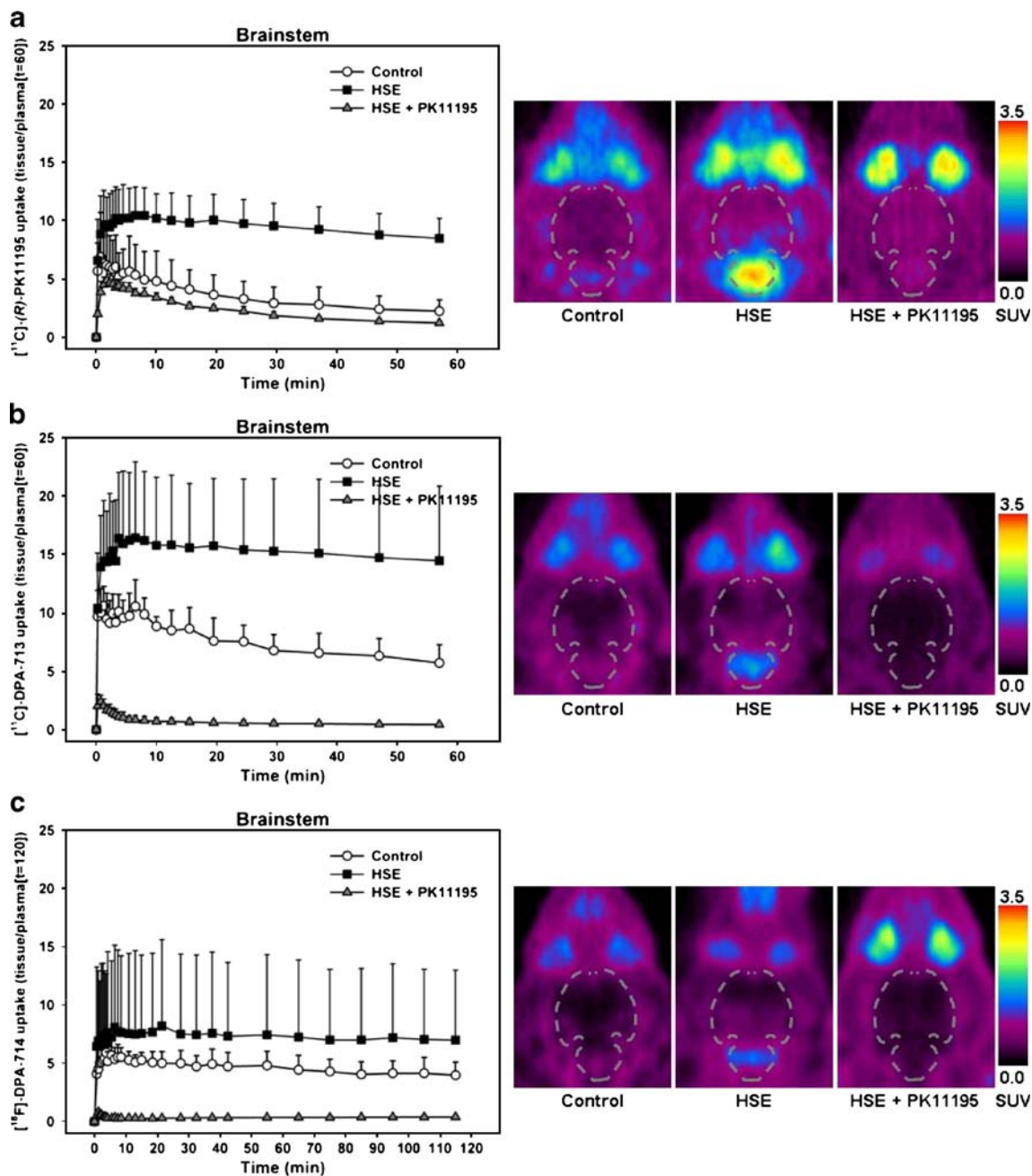
Fig. 3. Time–activity curves (*left*) of the brainstem for $[^{11}C]$-(R)-PK11195 (**a**), $[^{11}C]$-DPA-713 (**b**), and $[^{18}F]$-DPA-714 (**c**), and small animal PET images (*right*) of control rats (*control*), rats infected with HSV-1 (*HSE*), and rats infected with HSV-1 injected with 5 mg/kg PK11195 5 min before tracer injection (*HSE + PK11195*). The time–activity curves are expressed as tissue uptake divided by the ex vivo plasma uptake at $t=60$ for $[^{11}C]$-(R)-PK11195 and $[^{11}C]$-DPA-713, and at $t=120$ for $[^{18}F]$-DPA-714. Statistically significant differences are indicated by $*p<0.05$ and $†p<0.005$. The small animal PET images display a coronal plane of the rat head at the level of the brainstem, in which the brain is delineated by a *dashed line*. The images are summed images between 16 and 60 min for $[^{11}C]$-(R)-PK11195 and $[^{11}C]$-DPA-713, and between 12 and 120 min for $[^{18}F]$-DPA-714.

(R)-PK11195 in HSE rats, as compared to control rats, was found in the medulla (1.29 *vs.* 0.61, $p=0.004$), pons (1.54 *vs.* 0.59, $p<0.001$), and cerebellum (0.88 *vs.* 0.51, $p=0.001$). $[^{11}C]$-(R)-PK11195 binding to the TSPO was blocked by administration of unlabeled PK11195, resulting in a significantly

lower uptake of $[^{11}C]$-(R)-PK11195 in the medulla, pons, cerebellum, and bulbus olfactorius.

The ex vivo biodistribution of $[^{11}C]$-DPA-713 is shown in Table 3. As was found for $[^{11}C]$-(R)-PK11195, the bulbus olfactorius in HSE rats showed an increase in $[^{11}C]$-DPA-

Table 2. Ex vivo biodistribution of [^{11}C]-(R)-PK11195, expressed as standardized uptake values (SUV; mean ± SD), 60 min after tracer injection in control rats (control; $n=5$), rats infected with HSV-1 (HSE; $n=9$), and rats infected with HSV-1 pre-treated with 5 mg/kg PK11195 5 min before tracer injection (HSE + PK11195; $n=4$)

	Control	HSE	HSE + PK11195
Brain			
Amygdala/piriform cortex	0.37±0.11	0.40±0.11	0.49±0.08
Bulbus olfactorius	1.20±0.37	1.59±0.51	0.52±0.06****
Cerebellum	0.51±0.08	0.88±0.19**	0.49±0.07****
Cingulate/frontopolar cortex	0.31±0.05	0.48±0.20	0.47±0.06
Entorhinal cortex	0.33±0.07	0.41±0.12	0.46±0.07
Frontal cortex	0.33±0.08	0.40±0.13	0.51±0.06
Hippocampus	0.54±0.32	0.41±0.11	0.51±0.05
Medulla	0.61±0.12	1.29±0.42**	0.68±0.07***
Parietal/temporal/occipital cortex	0.33±0.08	0.40±0.10	0.51±0.06*
Pons	0.59±0.09	1.54±0.45**	0.67±0.08****
Striatum	0.31±0.06	0.40±0.13	0.53±0.04*
Peripheral tissues			
Adrenals	10.49±2.22	10.12±3.01	4.90±0.17*, ***
Bone	1.27±0.23	0.95±0.40	0.35±0.06*, ***
Lung	6.97±0.63	8.83±3.82	1.11±0.16****
Plasma	0.22±0.05	0.18±0.03	0.56±0.09**, ****

*$p<0.05$ as compared to control, **$p<0.005$ as compared to control, ***$p<0.05$ as compared to HSE, ****$p<0.005$ as compared to HSE

713 uptake when compared to control rats (1.30 $vs.$ 0.93), but this difference did not reach statistical significance. Uptake in the medulla (1.09 $vs.$ 0.46, $p=0.039$) and the pons (1.12 $vs.$ 0.46, $p=0.004$) of HSE rats was significantly elevated as compared to control rats. This was confirmed by blocking studies. Unlabeled PK11195 significantly reduced [^{11}C]-DPA-713 uptake in the bulbus olfactorius, pons, and medulla. The uptake of [^{11}C]-DPA-713 in control rats was on average 26% lower ($p<0.005$) than the uptake of [^{11}C]-(R)-PK11195, suggesting less non-specific binding. In addition, the brain uptake in PK11195 pre-treated rats was significantly lower for [^{11}C]-DPA-713 than for [^{11}C]-(R)-PK11195 ($p<0.005$).

[^{18}F]-DPA-714 uptake (Table 4) in control rats was significantly lower than [^{11}C]-(R)-PK11195 uptake (on average 41%, $p<0.005$). Significantly increased uptake of [^{18}F]-DPA-714 was found in the medulla of HSE rats (0.40 $vs.$ 0.81, $p=0.004$), when compared to control rats, while a non-significant increase in uptake was found in the bulbus olfactorius (0.55 $vs.$ 0.88). No effective blocking of [^{18}F]-DPA-714 uptake was found after administration of unlabeled PK11195.

Ex vivo biodistribution in peripheral organs showed a high uptake of [^{11}C]-(R)-PK11195, [^{11}C]-DPA-713, and [^{18}F]-DPA-714 in TSPO expressing organs, like the lungs and adrenals. In both the lungs and adrenals, [^{11}C]-(R)-

Table 3. Ex vivo biodistribution of [^{11}C]-DPA-713, expressed as standardized uptake values (SUV; mean ± SD), 60 min after tracer injection in control rats (control; $n=5$), rats infected with HSV-1 (HSE; $n=9$), and rats infected with HSV-1 pre-treated with 5 mg/kg PK11195 5 min before tracer injection (HSE + PK11195; $n=4$)

	Control	HSE	HSE + PK11195
Brain			
Amygdala/piriform cortex	0.31±0.09	0.36±0.19	0.24±0.12
Bulbus olfactorius	0.93±0.13	1.30±0.42	0.50±0.35***
Cerebellum	0.46±0.14	0.70±0.30	0.33±0.19
Cingulate/frontopolar cortex	0.17±0.04	0.32±0.22	0.40±0.44
Entorhinal cortex	0.20±0.05	0.33±0.19	0.23±0.10
Frontal cortex	0.23±0.16	0.26±0.15	0.25±0.18
Hippocampus	0.55±0.17	0.45±0.23	0.18±0.05*
Medulla	0.46±0.15	1.09±0.53*	0.31±0.17***
Parietal/temporal/occipital cortex	0.20±0.02	0.24±0.10	0.27±0.21
Pons	0.46±0.09	1.12±0.41**	0.28±0.08****
Striatum	0.16±0.02	0.28±0.15	0.18±0.04
Peripheral tissues			
Adrenals	5.10±1.19	5.75±1.79	8.01±2.35
Bone	0.83±0.24	0.69±0.33	0.48±0.12
Lung	10.68±1.41	13.80±4.14	1.06±0.37**, ****
Plasma	0.10±0.02	0.09±0.02	0.61±0.10**, ****

*$p<0.05$ as compared to control, **$p<0.005$ as compared to control, ***$p<0.05$ as compared to HSE, ****$p<0.005$ as compared to HSE

Table 4. Ex vivo biodistribution of [^{18}F]-DPA-714, expressed as standardized uptake values (SUV; mean ± SD), 120 min after tracer injection in control rats (control; $n=5$), rats infected with HSV-1 (HSE; $n=9$), and rats infected with HSV-1 pre-treated with 5 mg/kg PK11195 5 min before tracer injection (HSE + PK11195; $n=4$)

	Control	HSE	HSE + PK11195
Brain			
Amygdala/piriform cortex	0.25±0.08	0.41±0.34	0.50±0.17
Bulbus olfactorius	0.55±0.09	0.88±0.30	0.85±0.35
Cerebellum	0.36±0.05	0.41±0.20	0.43±0.08
Cingulate/frontopolar cortex	0.20±0.02	0.33±0.21	0.45±0.11
Entorhinal cortex	0.20±0.04	0.39±0.32	0.44±0.11
Frontal cortex	0.17±0.02	0.21±0.09	0.40±0.10**· ***
Hippocampus	0.35±0.25	0.39±0.16	0.48±0.14
Medulla	0.40±0.06	0.81±0.28*	0.45±0.08
Parietal/temporal/occipital cortex	0.17±0.02	0.19±0.05	0.38±0.09**· ***
Pons	0.31±0.02	0.58±0.26	0.43±0.09
Striatum	0.18±0.01	0.32±0.22	0.49±0.18
Peripheral tissues			
Adrenals	6.75±1.16	6.36±1.48	9.03±2.88
Bone	0.40±0.17	0.50±0.20	0.42±0.12
Lung	16.55±4.53	15.14±4.98	1.49±0.34**· ***
Plasma	0.13±0.02	0.22±0.34	1.15±0.35**· ***

*$p<0.05$ as compared to control, **$p<0.005$ as compared to control, ***$p<0.005$ as compared to HSE

PK11195 uptake was effectively blocked by unlabeled PK11195, resulting in a significant reduction in uptake, whereas the uptake of [^{11}C]-DPA-713 and [^{18}F]-DPA-714 was only significantly blocked in the lungs, but not in the adrenals.

Ex Vivo Biodistribution: Specific Binding

The ex vivo biodistribution showed an increased binding in HSE rats as compared to controls and a decreased binding after pre-treatment with PK11195, for all three PET tracers. However, plasma levels of the tracer were also found to be different between the three PET tracers and between treatment groups. Since tracer accumulation in the brain is dependent on tracer delivery (and thus tracer concentration) from plasma, the brain uptake was corrected for plasma radioactivity for each rat individually to calculate the tissue/plasma ratios.

Non-specific binding and specific binding of [^{11}C]-(R)-PK11195, [^{11}C]-DPA-713, and [^{18}F]-DPA-714 are displayed in Table 5. Non-specific binding was defined as the tissue/plasma ratio of rats pre-treated with PK11195. Specific binding was calculated in control and HSE rats, by subtracting the average tissue/plasma ratio of the HSE rats pre-treated with PK11195 from the tissue/plasma ratio of control and HSE rats, for each rat individually. The rationale behind the definition of specific uptake is that the uptake in rats pre-treated with PK11195 represents non-specific binding only, whereas the uptake in control and HSE rats is due to both specific and non-specific binding. Non-specific binding was found to be statistically significantly lower in almost all brain areas for both [^{11}C]-DPA-713 and [^{18}F]-DPA-714, when compared to [^{11}C]-(R)-PK11195. The specific binding in control rats was found to be significantly higher for [^{11}C]-

DPA-713 in the amygdala/piriform cortex, bulbus olfactorius, cerebellum, entorhinal cortex, medulla, parietal/temporal/ occipital cortex, pons, and striatum, when compared to [^{11}C]-(R)-PK11195. For [^{18}F]-DPA-714, the specific uptake in control rats was significantly higher than [^{11}C]-(R)-PK11195 uptake in the cingulate/frontopolar cortex, pons, and striatum. In addition, specific uptake in HSE rats was found to be significantly higher for [^{11}C]-DPA-713 in the amygdala/piriform cortex, bulbus olfactorius, entorhinal cortex, hippocampus, medulla, and parietal/temporal/occipital cortex as compared to [^{11}C]-(R)-PK11195. No significant differences in specific binding in HSE rats were found between [^{11}C]-(R)-PK11195 and [^{18}F]-DPA-714.

The specific binding in control rats showed a good correlation with [^{3}H]-PK11195 binding (Fig. 4) as was measured by Kurumaji et al. [25] for all three PET tracers. The best correlation was found for [^{11}C]-(R)-PK11195 that had a R of 0.96 ($p=0.0006$), followed by [^{11}C]-DPA-713 with a R of 0.87 ($p=0.01$) and [^{18}F]-DPA-714 with a R of 0.77 ($p=0.04$). Although the best correlation was found for [^{11}C]-(R)-PK11195, the slope of the linear regression was highest for [^{11}C]-DPA-713 (0.016; compared to 0.010 for [^{11}C]-(R)-PK11195 and 0.005 for [^{18}F]-DPA-714), which indicates that [^{11}C]-DPA-713 uptake might be most sensitive to changes in TSPO expression. Although these results seem to depend on the bulbus olfactorius, which has the highest uptake, the correlation remained good after removal of this data point from the regression analysis. In addition, the slope of the linear regression remained highest for [^{11}C]-DPA-713.

Discussion

In the present study, the new TSPO ligands [^{11}C]-DPA-713 and [^{18}F]-DPA-714 were evaluated in a rat model of herpes

Table 5. Non-specific and specific binding of $[^{11}C]$-(R)-PK11195, $[^{11}C]$-DPA-713, and $[^{18}F]$-DPA-714

	$[^{11}C]$-(R)-PK11195	$[^{11}C]$-DPA-713	$[^{18}F]$-DPA-714
Non-specific binding			
Amygdala/piriform cortex	0.88±0.05	0.39±0.18*	0.47±0.21*
Bulbus olfactorius	0.94±0.11	0.81±0.53	0.80±0.40
Cerebellum	0.89±0.11	0.53±0.29	0.40±0.12*
Cingulate/frontopolar cortex	0.85±0.08	0.64±0.67	0.42±0.16
Entorhinal cortex	0.84±0.11	0.38±0.15**	0.41±0.15*
Frontal cortex	0.91±0.07	0.41±0.27*	0.37±0.13*
Hippocampus	0.93±0.10	0.30±0.06**	0.45±0.18**
Medulla	1.23±0.15	0.50±0.26**	0.41±0.13**
Parietal/temporal/occipital cortex	0.91±0.10	0.44±0.31*	0.35±0.13*
Pons	1.21±0.10	0.46±0.14**	0.40±0.14**
Striatum	0.97±0.10	0.30±0.04**	0.46±0.21**
Specific binding control			
Amygdala/piriform cortex	0.69±0.64	2.62±0.71*	1.44±0.62
Bulbus olfactorius	4.64±2.22	8.28±1.37**	3.43±0.82
Cerebellum	1.50±0.73	3.90±1.20**	2.47±0.82
Cingulate/frontopolar cortex	0.57±0.26	1.06±0.35	1.12±0.25*
Entorhinal cortex	0.67±0.42	1.62±0.45**	1.20±0.62
Frontal cortex	0.57±0.29	1.85±1.62	0.96±0.35
Hippocampus	1.81±2.26	5.02±1.38	2.37±2.38
Medulla	1.56±0.70	3.93±1.45**	2.76±0.75
Parietal/temporal/occipital cortex	0.57±0.31	1.48±0.21*	1.00±0.38
Pons	1.51±0.72	4.05±0.81*	2.07±0.54
Striatum	0.46±0.27	1.22±0.15*	0.95±0.29*
Specific binding HSE			
Amygdala/piriform cortex	1.38±0.63	3.87±2.58*	2.14±0.80
Bulbus olfactorius	8.39±3.64	14.44±5.66*	6.89±2.45
Cerebellum	4.36±1.85	7.72±3.68	3.66±2.80
Cingulate/frontopolar cortex	1.89±1.02	3.23±2.99	1.98±0.47
Entorhinal cortex	1.55±0.71	3.54±2.52*	2.09±0.46
Frontal cortex	1.37±0.59	2.64±2.01	1.30±0.28
Hippocampus	1.44±0.62	4.99±2.88**	3.01±0.79
Medulla	6.21±2.22	12.56±7.11*	7.18±3.90
Parietal/temporal/occipital cortex	1.37±0.40	2.44±1.37*	1.24±0.34
Pons	7.77±2.87	12.77±5.39	5.03±3.67
Striatum	1.39±0.98	3.06±2.07	1.80±0.50

Non-specific binding was defined as the tissue/plasma ratio of HSE rats pre-treated with PK11195 ($n=4$). The specific binding in control ($n=5$) and HSE ($n=9$) rats were calculated by the equations [control$_{tissue/plasma}$ − average pre-treated$_{tissue/plasma}$] and [HSE$_{tissue/plasma}$ − average pre-treated$_{tissue/plasma}$], respectively
*$p<0.05$ and **$p<0.005$ as compared to $[^{11}C]$-(R)-PK11195
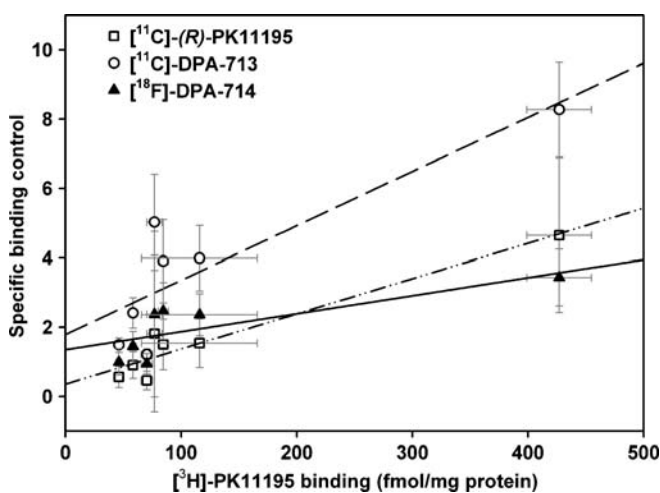
Fig. 4. Correlation of specific binding in control rats for $[^{11}C]$-(R)-PK11195, $[^{11}C]$-DPA-713, and $[^{18}F]$-DPA-714 with $[^{3}H]$-PK11195 binding as determined by Kurumaji et al. [25]. The R was 0.96 for $[^{11}C]$-(R)-PK11195 ($p=0.0006$; $y=0.36+0.010x$), 0.87 for $[^{11}C]$-DPA-713 ($p=0.0116$; $y=1.79+0.016x$), and 0.77 for $[^{18}F]$-DPA-714 ($p=0.0427$; $y=1.35+0.005x$).

encephalitis, using small animal PET imaging. We demonstrated that $[^{11}C]$-DPA-713 has lower background binding and has the potency to reach higher specific uptake in infected brain tissue than $[^{11}C]$-(R)-PK11195. $[^{18}F]$-DPA-714 showed low non-specific binding, but also lower specific binding. Data from immunohistochemistry, in vivo PET imaging, and ex vivo biodistribution corresponded nicely for all tracers.

The TSPO that is only modestly expressed in the healthy brain is upregulated in microglia cells when they become activated in response to inflammatory stimuli and brain damage. Microglia cells are increasingly associated with neurological diseases, such as Parkinson's disease [15] and multiple sclerosis [9], and are therefore an important target for early diagnosis and detection of the subtle effects of therapeutic intervention. At present, the most widely used PET tracer to visualize activated microglia is the TSPO ligand $[^{11}C]$-(R)-PK11195, but this radiotracer may not provide the required sensitivity. The high lipophilicity and high non-specific binding of $[^{11}C]$-(R)-PK11195 result in a low signal-to-noise ratio, which makes detecting mild

neuroinflammation or subtle changes due to treatment difficult.

The majority of studies that evaluate new radioligands for the TSPO use striatum-lesioned models of neuroinflammation, in which a toxic substance, like quinolinic acid, kainic acid, or 6-OH-DOPA, is stereotactically injected into the striatum. The rat model of herpes encephalitis better mimics neurological disorders as it does not involve invasive manipulations, but induces microglia cell activation via a biological process. In addition, HSV-1 is implicated in the etiopathogenesis of neurological and psychiatric disorders, like schizophrenia [26] and Alzheimer's disease [26, 27] and may be specifically involved in the focal neuroinflammatory processes in these disorders. It has already been shown that HSV-1 invasion of the brain is associated with the activation of microglia cells [13, 28, 29]. Also in the present study, it was confirmed by immunohistochemical staining that the central nervous system invasion of HSV-1 results in intense microglia activation, in the bulbus olfactorius, frontal cortex, hippocampus, cerebellum, and brainstem. The pattern of this microglia activation is consistent with the findings of Barnett et al. [30], who showed that intranasal inoculation of mice with HSV-1 resulted in the spread of HSV-1 to the hippocampus, amygdala, midbrain, and brainstem via the olfactory bulb. The severe activation of microglia cells in the brainstem may be caused by indirect HSV-1 invasion of the brainstem via the neural pathway from the bulbus olfactorius to the locus coeruleus [30, 31] or by direct invasion of the sensory trigeminal nuclei via the main sensory nerve of the face, the trigeminal nerve. In addition, microglia cell activation in the brainstem may also be caused by HSV-1 invasion of the trigeminal nerve, resulting in activation of microglia cells surrounding the anterograde nerve connections [32]. Although the rat model of herpes encephalitis represents a more physiological model of microglia activation, a disadvantage of the model compared to striatum lesion models is the variability in the extent of microglia activation. Despite the variation in the extent of microglia cell activation, it was shown that the brainstem was affected in all rats. One way to reduce some variation in measurement of microglia cell activation would be to compare the different PET tracers in the same rat. However, due to the severity of the disease, the degree of microglia cell activation can change quickly within the time period between the PET scans which makes it difficult compare the tracers in the same rat.

The uptake of $[^{11}C]$-(R)-PK11195, $[^{11}C]$-DPA-713, and $[^{18}F]$-DPA-714 was determined by both PET scanning and ex vivo biodistribution. Uptake values derived from the PET scan were on average higher than the values obtained from ex vivo biodistribution, but this difference was statistically not significant. The small difference between both techniques can probably be attributed to tissue kinetics, since the ex vivo biodistribution represents a single time point, whereas the values obtained from the PET scan represent an average of 10 min. In regions with a high uptake and thus slower washout, like the bulbus olfactorius, this results in PET values lower than the ex vivo biodistribution values. For brain regions with lower uptake and faster washout, and thus a larger change within 10 min, this results in PET values that are lower or equal to the ex vivo biodistribution values.

In the present study, it was shown that the standardized uptake value of $[^{11}C]$-DPA-713 is significantly lower in healthy brain tissue as compared to the uptake of $[^{11}C]$-(R)-PK11195. This suggests less non-specific binding. Indeed, pre-treatment with PK11195 showed that $[^{11}C]$-DPA-713 has lower non-specific binding than $[^{11}C]$-(R)-PK11195. This could be explained by the lower lipophilicity of DPA-713 than that of PK11195 (LogP 2.4 vs. 3.4 [22]). In brain areas in HSV-infected animals where activation of microglia cells was found, $[^{11}C]$-DPA-713 uptake was comparable to the uptake of $[^{11}C]$-(R)-PK11195. Thus, the lower non-specific binding and comparable uptake in infected areas results in a higher signal-to-noise ratio of $[^{11}C]$-DPA-713 than of $[^{11}C]$-(R)-PK11195, suggesting that $[^{11}C]$-DPA-713 is more suitable for the detection of mild neuroinflammation. The results of the present study are consistent with the findings of Boutin et al. [23]. In their study, it was also shown that the signal-to-noise ratio of $[^{11}C]$-DPA-713 is higher than that of $[^{11}C]$-(R)-PK11195, due to a reduced uptake in healthy tissue for $[^{11}C]$-DPA-713.

In healthy brain tissue, the standardized uptake value of $[^{18}F]$-DPA-714 is significantly lower than the uptake of both $[^{11}C]$-(R)-PK11195 and $[^{11}C]$-DPA-713. In addition, the non-specific binding of $[^{18}F]$-DPA-714 was found to be lower than the non-specific $[^{11}C]$-(R)-PK11195 binding. This suggests that this radiotracer is potentially suitable for visualizing mild neuroinflammation. Although $[^{18}F]$-DPA-714 is able to visualize neuroinflammation in our rat model of herpes encephalitis and also in a striatum-lesioned model [19, 20], the uptake in infected brain areas is significantly lower as compared to $[^{11}C]$-(R)-PK11195.

Although the standardized uptake value is widely used to display the uptake of tracers, it does not correct for the activity in plasma, and thus, not for tracer delivery to the brain. This could lead to a wrong interpretation of the data when comparing the tracers in different conditions. Ideally, the binding potential or distribution volume of the tracers should be determined using plasma input on different time points during the scan. However, plasma samples are difficult to obtain, especially in severely ill animals. Therefore, in the present study, the tissue/plasma ratios were calculated from a single ex vivo plasma activity measurement. After correction for plasma activity, the specific binding in both control and HSE rats was found to be significantly higher for $[^{11}C]$-DPA-713 than for $[^{11}C]$-(R)-PK11195. In contrast to $[^{11}C]$-(R)-PK11195, $[^{11}C]$-DPA-713 is even able to show specific binding to the low basal expression levels of TSPO in control rats. In addition, the greater slope of the correlation between tracer uptake and TSPO expression (Fig. 4) suggests that $[^{11}C]$-DPA-713 is more sensitive for small changes in the amount of TSPO as compared to $[^{11}C]$-(R)-PK11195. Thus, this study indicates that $[^{11}C]$-DPA-713 is more sensitive for visualizing neuroinflammation than $[^{11}C]$-(R)-PK11195.

Although [^{18}F]-DPA-714 showed low non-specific binding, specific binding of [^{18}F]-DPA-714 was much lower than that of [^{11}C]-DPA-713, even after correction for plasma activity. Interestingly, a recent study in a striatum lesion model showed that the tissue uptake ratio between the control and lesioned striatum was higher for [^{18}F]-DPA-714 than for [^{11}C]-(R)-PK11195, with three times higher binding potential of [^{18}F]-DPA-714 [33]. Moreover, in the present study, [^{18}F]-DPA-714 binding (SUV) in infected brain areas was not effectively blocked by pre-treatment with PK11195, while [^{18}F]-DPA-714 uptake in the striatum lesion model was inhibited by pre-treatment with PK11195, DPA-713, and DPA-714 [20, 22]. The apparent discrepancy between the results of our study and those of the previous studies in the striatum lesion model might be due to differences in the affinity state of the receptor between both animal models. [^{18}F]-DPA-714 is an agonist of the TSPO and an agonist usually binds only to the high affinity state of the receptor. Microglia cell activation in the striatum lesion model has a more chronic, neurodegenerative character, as microglia cells are mainly involved in removing the debris of the neuronal cells that were destroyed by the chemical compound. In the HSE model, the activated microglia cells are involved in a more acute response by combating the exogenous pathogen and thus they have a more neuroprotective role. One could speculate that the affinity state of the TSPO depends on the neuroprotective or neurodegenerative activity of the microglia cells. The chronically activated (neurodenerative) microglia cells may contain more TSPO in the high affinity state, which would result in better binding of [^{18}F]-DPA-714. If this hypothesis could be confirmed, TSPO, agonists like [^{18}F]-DPA-714, may be important radiotracers to visualize an important aspect of neuroinflammation.

Another remarkable finding in this study was that the binding of [^{18}F]-DPA-714 and [^{11}C]-DPA-713 in the adrenals could not be blocked by pre-treatment with PK11195, whereas pre-treatment did block the binding of [^{11}C]-(R)-PK11195. For [^{18}F]-DPA-714, similar results were found by James et al. [19, 20]. This observation suggests the presence of an alternative binding site for DPA-713 and DPA-714 that is predominantly expressed in the adrenals and does not bind PK1115. Whether the alternative binding site in the adrenals could be a hitherto unknown subtype of the TSPO, or another receptor, remains to be elucidated.

Conclusion

The present results showed that [^{11}C]-DPA-713 is a promising new radioligand for TSPO expression in activated microglia due to its low non-specific binding in the brain. This tracer appears to be a more sensitive tool to detect small changes in TSPO expression than [^{11}C]-(R)-PK11195. To validate superiority of [^{11}C]-DPA-713 over [^{11}C]-(R)-PK11195 in quantification of neuroinflammation, clinical studies in neurological diseases that are associated with

microglia cell activation are needed. Although there may be differences in the affinity state of the TSPO between previous animal models using [^{18}F]-DPA-714 and the present study, the fact that this radioligand is an agonist of the TSPO may open new possibilities in PET imaging of neuroinflammation, which warrants its further evaluation.

References

1. World Health Organization (2006) Neurological disorders; public health challenges. WHO, Geneva
2. Nakajima K, Kohsaka S (2004) Microglia: neuroprotective and neurotrophic cells in the central nervous system. Curr Drug Targets Cardiovasc Haematol Disord 4(1):65–84
3. Davalos D, Grutzendler J, Yang G et al (2005) ATP mediates rapid microglial response to local brain injury *in vivo*. Nat Neurosci 8(6):752–758
4. Nimmerjahn A, Kirchhoff F, Helmchen F (2005) Resting microglial cells are highly dynamic surveillants of brain parenchyma *in vivo*. Science 308(5726):1314–1318
5. Gerhard A, Neumaier B, Elitok E et al (2000) *In vivo* imaging of activated microglia using [11C]PK11195 and positron emission tomography in patients after ischemic stroke. Neuroreport 11 (13):2957–2960
6. Gerhard A, Schwarz J, Myers R, Wise R, Banati RB (2005) Evolution of microglial activation in patients after ischemic stroke: a [11C](R)-PK11195 PET study. Neuroimage 24(2):591–595
7. Pappata S, Levasseur M, Gunn RN et al (2000) Thalamic microglial activation in ischemic stroke detected *in vivo* by PET and [11C] PK1195. Neurology 55(7):1052–1054
8. Ramsay SC, Weiller C, Myers R et al (1992) Monitoring by PET of macrophage accumulation in brain after ischaemic stroke. Lancet 339 (8800):1054–1055
9. Banati RB, Newcombe J, Gunn RN et al (2000) The peripheral benzodiazepine binding site in the brain in multiple sclerosis: quantitative *in vivo* imaging of microglia as a measure of disease activity. Brain 123:2321–2337
10. Debruyne JC, Versijpt J, Van Laere KJ et al (2003) PET visualization of microglia in multiple sclerosis patients using [11C]PK11195. Eur J Neurol 10(3):257–264
11. Versijpt J, Debruyne JC, Van Laere KJ et al (2005) Microglial imaging with positron emission tomography and atrophy measurements with magnetic resonance imaging in multiple sclerosis: a correlative study. Mult Scler 11(2):127–134
12. Vowinckel E, Reutens D, Becher B et al (1997) PK11195 binding to the peripheral benzodiazepine receptor as a marker of microglia activation in multiple sclerosis and experimental autoimmune encephalomyelitis. J Neurosci Res 50(2):345–353
13. Cagnin A, Myers R, Gunn RN et al (2001) *In vivo* visualization of activated glia by [11C] (R)-PK11195-PET following herpes encephalitis reveals projected neuronal damage beyond the primary focal lesion. Brain 124(Pt 10):2014–2027
14. Gerhard A, Pavese N, Hotton G et al (2006) *In vivo* imaging of microglial activation with [11C](R)-PK11195 PET in idiopathic Parkinson's disease. Neurobiol Dis 21(2):404–412

15. Ouchi Y, Yoshikawa E, Sekine Y et al (2005) Microglial activation and dopamine terminal loss in early Parkinson's disease. Ann Neurol 57 (2):168–175

16. Cagnin A, Brooks DJ, Kennedy AM et al (2001) *In-vivo* measurement of activated microglia in dementia. Lancet 358(9280):461–467

17. Cagnin A, Rossor M, Sampson EL, Mackinnon T, Banati RB (2004) In vivo detection of microglial activation in frontotemporal dementia. Ann Neurol 56(6):894–897

18. Groom GN, Junck L, Foster NL, Frey KA, Kuhl DE (1995) PET of peripheral benzodiazepine binding sites in the microgliosis of Alzheimer's disease. J Nucl Med 36(12):2207–2210

19. James ML, Fulton RR, Vercouille J et al (2007) DPA-714 a new translocator protein (18 kDa) ligand: synthesis, radiofluorination and pharmacological characterisation. J Label Compd Radiopharm 50 (Supplement 1):S25

20. James ML, Fulton RR, Vercoullie J et al (2008) DPA-714, a new translocator protein-specific ligand: synthesis, radiofluorination, and pharmacologic characterization. J Nucl Med 49(5):814–822

21. Selleri S, Bruni F, Costagli C et al (2001) 2-Arylpyrazolo[1,5-a] pyrimidin-3-yl acetamides. New potent and selective peripheral benzodiazepine receptor ligands. Bioorg Med Chem 9(10):2661–2671

22. James ML, Fulton RR, Henderson DJ et al (2005) Synthesis and *in vivo* evaluation of a novel peripheral benzodiazepine receptor PET radioligand. Bioorg Med Chem 13(22):6188–6194

23. Boutin H, Chauveau F, Thominiaux C et al (2007) 11C-DPA-713: a novel peripheral benzodiazepine receptor PET ligand for *in vivo* imaging of neuroinflammation. J Nucl Med 48(4):573–581

24. Larsen P, Ulin J, Dahlstrom K, Jensen M (1997) Synthesis of [C-11] iodomethane by iodination of [C-11]methane. Appl Radiat Isot 48 (2):153–157

25. Kurumaji A, Kaneko K, Toru M (1996) Effects of chronic treatment with haloperidol on [3H]PK 11195 binding in the rat brain and peripheral tissues. Neuropharmacology 35(8):1075–1079

26. Steiner J, Mawrin C, Ziegeler A et al (2006) Distribution of HLA-DR-positive microglia in schizophrenia reflects impaired cerebral lateralization. Acta Neuropathol 112(3):305–316

27. Itzhaki R (2004) Herpes simplex virus type 1, apolipoprotein E and Alzheimer' disease. Herpes 11(Suppl 2):77A–82A

28. DeLano RM, Mallery SR (1998) Stress-related modulation of central nervous system immunity in a murine model of herpes simplex encephalitis. J Neuroimmunol 89(1–2):51–58

29. Esiri MM, Drummond CW, Morris CS (1995) Macrophages and microglia in HSV-1 infected mouse brain. J Neuroimmunol 62(2):201–205

30. Barnett EM, Cassell MD, Perlman S (1993) Two neurotropic viruses, herpes simplex virus type 1 and mouse hepatitis virus, spread along different neural pathways from the main olfactory bulb. Neuroscience 57(4):1007–1025

31. Mori I, Goshima F, Ito H et al (2005) The vomeronasal chemosensory system as a route of neuroinvasion by herpes simplex virus. Virology 334(1):51–58

32. Banati RB (2002) Visualising microglial activation *in vivo*. Glia 40 (2):206–217

33. Chauveau F, van Camp N, Damont A et al (2008) [^{18}F]DPA-714: a highly promising fluorine-18-labelled tracer for neuroinflammation imaging. World Molecular Imaging Congress